Bulletin of Pure and Applied Science
Physics, Vol.45D No.1,
January-June 2026 P.35-50
Original Research Article

Print version ISSN 0970 6569
Online version ISSN 2320 3218
Available online at www.bpasjournals.com

Exploring the Synthesis of Zinc Oxide Nanoparticles Employing Different Techniques and change in Dielectric Constant in Composite (PVC/ZnO-A and PVC/ZnO-B) at Various Temperatures and Concentrations

[1]Aman Kumar*, [2]Kamar Tanbir, [3]Sanjeev Kumar, [4]Sanjay Kumar Yadav, [5]Rakesh Kumar Singh, [6]N.A. Karimi

Author's Affiliations:

[1]*Department of Physics, Patna Science College, Patna University, Patna
[2] Maulana Azad College of Engineering and Technology, Neora, Patna
[3] Department of Physics, IIT BHU, Varanasi
[4] Department of Chemistry, Patna Science College, Patna University, Patna
[5] Department of Nano-Science and Nanotechnology AKU, Patna
[6] Department of Physics, B.N. College, Patna University, Patna

***Corresponding author:**

Aman Kumar
Department of Physics, Patna Science College, Patna University, Patna
E-mail: dr.amanpu@gmail.com

ABSTRACT

Two sol-gel techniques were used to create zinc oxide (ZnO) nanoparticles: nanoparticles ZnO-A were created by carefully adding a homogeneous solution of sodium hydroxide dropwise into a homogeneous solution of zinc sulphate, whereas nanoparticles ZnO-B were created by abruptly adding a homogeneous solution of sodium hydroxide into a homogeneous solution of zinc sulphate. Heat treatment was used to create powdered zinc oxide, ZnO-A and ZnO-B nanoparticles, which were then analyzed by Dynamic Light Scattering (DLS), and demonstrated that how the enhanced mobility of tiny particles affects the light scattering patterns. The stability of zinc oxide (ZnO-A) nanoparticles was evaluated using sophisticated method such as Nanoparticle Tracking Analysis (NTA) and Zeta Potential studies, which demonstrated its higher stability with a Zeta Potential of 55.98 mV as opposed to ZnO-B nanoparticles having Zeta potential 30.39 mV. The dielectric behavior of the composite (PVC/ZnO-A or PVC/ZnO-B) reveals unique performance traits, impacted by the nanoparticle properties, offering information for applications across a range of technological domains.

KEYWORDS

Nanoparticles, DLS, NTA, PVC, dielectric constant, Temperatures.

Received on 27.02.2026, Revised on 24.04.2026, Accepted on 17.06.2026

How to cite this article: Kumar A., Tanbir K., Kumar S., Yadav S.K., Singh R.K., Karimi N.A. Exploring the Synthesis of Zinc Oxide Nanoparticles Employing Different Techniques and change in Dielectric Constant in Composite (PVC/ZnO-A and PVC/ZnO-B) at Various Temperatures and Concentrations. *Bulletin of Pure and Applied Sciences- Physics,* 2026;45D (1): 35-50.

INTRODUCTION

Zinc oxide (ZnO), a naturally occurring substance with a wide gap of 3.37 eV and an excitation binding energy of 60 MeV, has been widely used in a variety of scientific field, including physics, chemistry, biochemistry, medical science, material science, solid state electronics etc., primarily because of its distinctive physical and chemical characteristics (such as a wide range of radiation absorption, high chemical stability, high photostability and high electrochemical coupling coefficient) [1, 2]. Zinc oxide (ZnO) is an n-type group II-VI semiconductor, because zinc belongs to the 2nd group, while oxygen belongs to the 6th group of the periodic table. It is used as an additive in a plethora of materials and products like plastics, ceramics, rubber, cement, pigments, batteries, glass, adhesives, paints, ointments, lubricants, ferrites, sealants, and fire retardants. The variations in the physical and chemical properties of zinc oxide (ZnO) nanoparticles can be tuned by changing the morphology using various synthesis routes [3]. In addition, it has high electron mobility, high thermal and mechanical stability at room temperature, good transparency, a broad range of radiation absorption, strong room temperature luminescence, and high photostability, that makes zinc oxide (ZnO) nanoparticles for multitasking material applications [4, 5]. It is seen as a promising material in the film of piezoelectric, transparent electronic, spintronic, photovoltaic, sensing, and optoelectronic devices. Due to antimicrobial and antitumor activity, it is used in human medicine as an astringent and to treat haemorrhoids, eczema, and excoriation [6]. Because of its large band gap of 3.37 eV, nanoparticles zinc oxide (ZnO-A and ZnO-B) can be used as a light-emitting diode, photodetector in sensors and the devices that produce a surface acoustic wave. However, they are cytotoxic to highly proliferating cells because they produce more ROS (reactive oxygen species) [7, 8]. The Nanoparticle Tracking Measurement (NTA) measured the size distribution, surface charge, quantity, and concentration of particles in liquid suspension by tracking Brownian motion in real time, whereas Dynamic Light Scattering (DLS) quantifies the hydrodynamic particle size distribution and stability [9]. Using an LCR meter, the capacitance was measured at different frequencies, and then the dielectric constants of composites (PVC/ZnO-A and PVC/ZnO-B) with the variation of temperatures and frequencies were measured. The endeavor intends to boost electrical conductivity, which is more beneficial for the manufacturer of electrical equipment since more electrons on the surface will contribute to the creation of electrical conductivity.

EXPERIMENTAL

For the preparation of zinc oxide (ZnO) nanoparticles by the sol-gel method using two different routes, a homogeneous solution of zinc sulphate (Chemical Corporation of India) and another homogeneous solution of sodium hydroxide (Merck Specialties Private Ltd., India) were mixed. In the first way, the sodium hydroxide solution was added dropwise to the zinc sulphate solution at regular intervals of time with continuous stirring. The obtained solution was filtered using whatman filter paper and rinsed with deionized water to remove all the sulphate ions [10]. In this way, a residue of produced zinc hydroxide is put on a glass substrate, and placed in an oven for alternating warming and chilling. After warming at 150°C for an hour and cooling for half an hour five times, a sample of zinc oxide nanoparticles was obtained as ZnO-A in powder form. In a similar manner, the second method involved abruptly adding the prepared sodium hydroxide solution to the prepared zinc sulphate solution, but with stirring constantly for 72 hours. The residue out on a glass substrate was warmed alternately in an oven and cooled, after being cleaned and removing the sulphate ions. Zinc oxide nanoparticles were produced as ZnO-B in powder form after five cycles of warming and chilling using a similar procedure [11, 12].

Flow chart for the synthesis of Zinc Oxide (ZnO) Nanoparticles by Conventional Precipitation Method:

$ZnSo_4 + 2NaOH = Zn(OH)_2 + Na_2So_4$; $Zn(OH)_2 \xrightarrow{Warming}$ $ZnO + H_2O$ (Vapour)

9.67 gm Zinc Sulphate + 40 cm^3 distilled water = Zinc Sulphate solution

1.61 gm Sodium Hydroxide + 120 cm^3 distilled water = Sodium Hydroxide solution

Zinc Sulphate solution + Sodium Hydroxide solution $\xrightarrow{Dropwise\ method\ of\ mixing}$ Zinc Hydroxide Solution - (A)

Zinc Hydroxide Solution - (B) $\xrightarrow{Heating\ and\ Cooling\ at\ 150^oC}$ ZnO-B (powder)

Zinc Hydroxide Solution - (A) $\xrightarrow{Heating\ and\ Cooling\ at\ 150^oC}$ ZnO-A (powder)

Zinc Sulphate solution + Sodium Hydroxide solution $\xrightarrow{Abruptly\ blended}$ Zinc Hydroxide Solution ----------(B)

RESULT AND DISCUSSION

Characterization through Dynamic Light Scattering (DLS):

Dynamic light scattering (DLS), a technique for measuring particle size, intensity, number distribution, and volume-mass distribution using Zetasizer software, reports the particle size and quantity of aggregation. Brownian motion of particles in suspension provides the basis for measuring the size distribution of zinc oxide nanoparticles using a Dynamic Light Scattering (DLS) cum Zeta Potential Analyzer (Micromeritics Instruments Corp., USA) [13]. To measure the particle size of the nanoparticles, they are dispersed in a solvent (deionized or Milli-Q water), and a homogeneous solution is prepared. Particles having a small size move faster than the larger-sized particles, and the light scattered by these particles, as observed in dynamic light scattering, provides information about the diffusion speed and the particle size distribution [14]. Larger particles scatter more light than smaller ones because they scatter all visible light wavelengths, but smaller particles can scatter shorter wavelengths more effectively. Light is scattered more symmetrically by smaller particles and more forwardly by larger ones [15].

Particle Size distribution:

The Stokes-Einstein equation for Brownian motion provides information about the particle size in terms of temperature, viscosity, and diffusion rate, which is given by the equation.

$$x = \frac{BT}{3\pi\mu\Delta}$$

Where T is the temperature, B is the Boltzmann constant, x is the particle diffusion coefficient, μ is the coefficient of viscosity, and Δ is the particle's hydrodynamic diameter, which is marginally bigger than the particle's average diameter [16].

Characterization through Nanoparticle Tracking Analysis (NTA):

Nanoparticle Tracking Analysis (NTA), which allows for the simultaneous measurement of particle size and particle concentration in liquid suspension, is based on the premise of tracking the

Brownian motion of individual particles in the liquid suspension rather than their scattering light, and it attributes the motion to particle size. By counting the number of particles in the observed volume, the NTA software analyzes particle movement and determines particle size based on diffusion rate and particle concentration. It can access lower particle concentration and provide superior results for polydisperse samples.

Both DLS and NTA rely on Brownian motion and light scattering; NTA focuses on particle-by-particle analysis, whereas DLS is intensity-based and necessitates high concentrations of particles with high scattering cross-sections [17]. FTLA (Finite Track Length Adjustment), ideal for monodisperse and bimodal mixtures, is a statistical technique used in NTA to track data in order to increase the accuracy of size distribution by adjusting for the influence caused by the short tracking length of particles, in terms of the number of particles per milliliter (particles/ml) [18]. The narrower peaks in nanoparticle tracking analysis (NTA), which display discrete populations of nanoparticles with similar hydrodynamic diameters as calculated by their Brownian motion using the Stokes-Einstein equation, are the outcome of FTLA (Finite Track Length Adjustment). The different peaks in FTLA (Finite Track Length Adjustment) analysis for polydisperse particles show distinct size populations within the sample's particle size distribution.

In the fluorescence mode of Nanoparticle Tracking Analysis (NTA), different signals from tagged nanoparticles are isolated employing filters (long-pass or bandpass optical) that allow fluorescent emission to pass through for detection while blocking the excitation laser wavelength.

The analysis of the sample under scatter mode (no filter) shows a model distribution at 61 nm with a fine concentration shown in figures 1 and 2 for solvent dispersed with (ZnO-A) nanoparticles, and figures 3 and 4 for solvent dispersed with (ZnO-B) nanoparticles. In contrast, under fluorescence mode, the distribution of the labelled population shows the same when a longer pass filter is inserted, confirming that the sample is free of impurities.

In figures 1 and 2, shown, NTA measured the distribution of particle sizes as well as the absolute particle concentration between 61 nm and 490 nm. The sizes of the different particle's populations are to be 61 nm, 126 nm, 197 nm, 265 nm, and 374 nm, which are identified on the graph's peaks. In figures 3 and 4, the measurement focuses on particle sizes ranging from 61 nm to 460 nm and the peaks 61 nm, 133 nm, 216 nm, and 460 nm are observed on the nanometer scale.

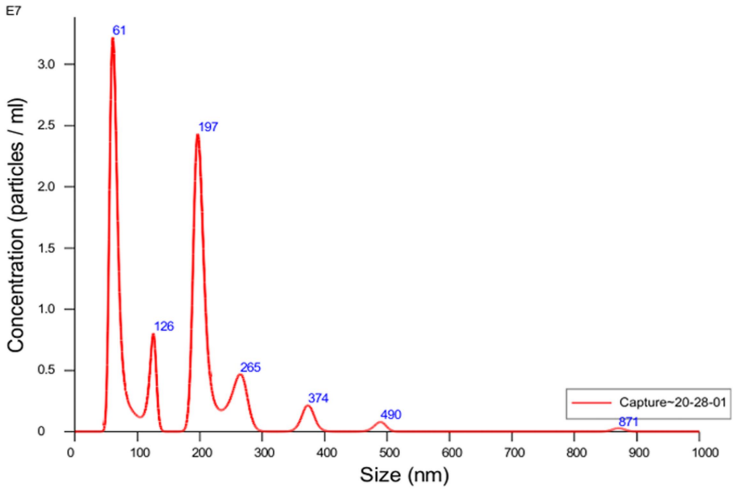

Figure 1: (Finite track length adjustment (FTLA) concentration/size image for ZnO-A, nanoparticle tracking analysis (NTA)) with no Filter

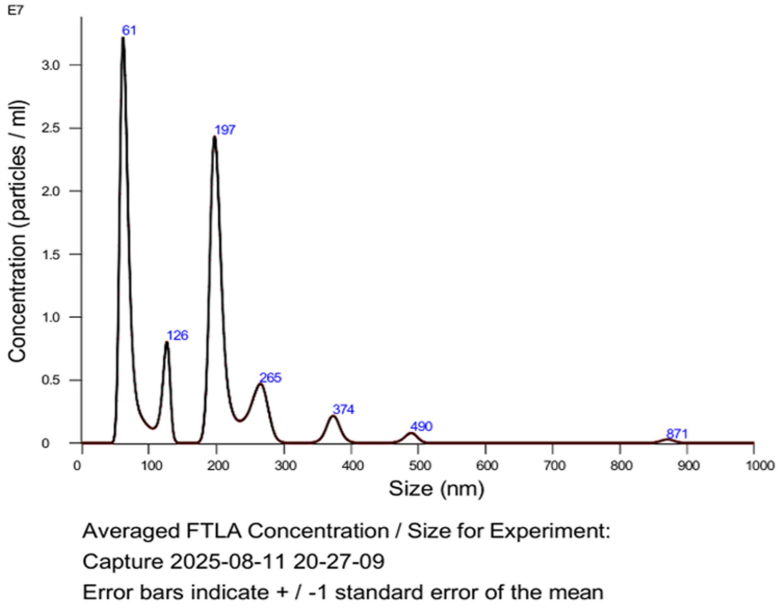

Figure 2: (Finite track length adjustment (FTLA) concentration/size image for ZnO-A, nanoparticle tracking analysis (NTA)) with Filter

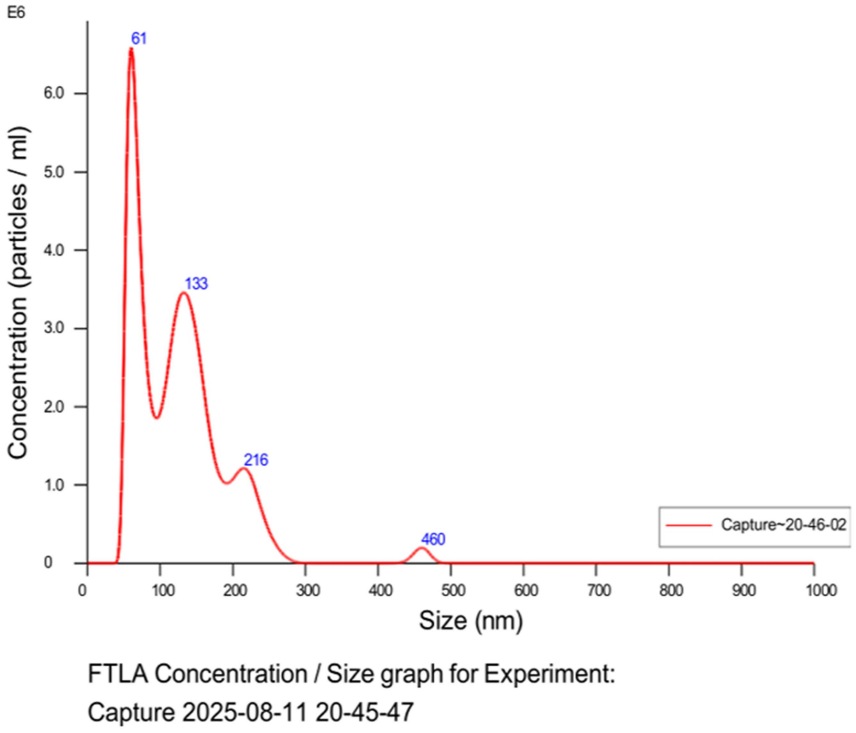

Figure 3: (Finite track length adjustment (FTLA) concentration/size image for nanoparticle tracking analysis (NTA) ZnO-B Nanoparticle) with no Filter

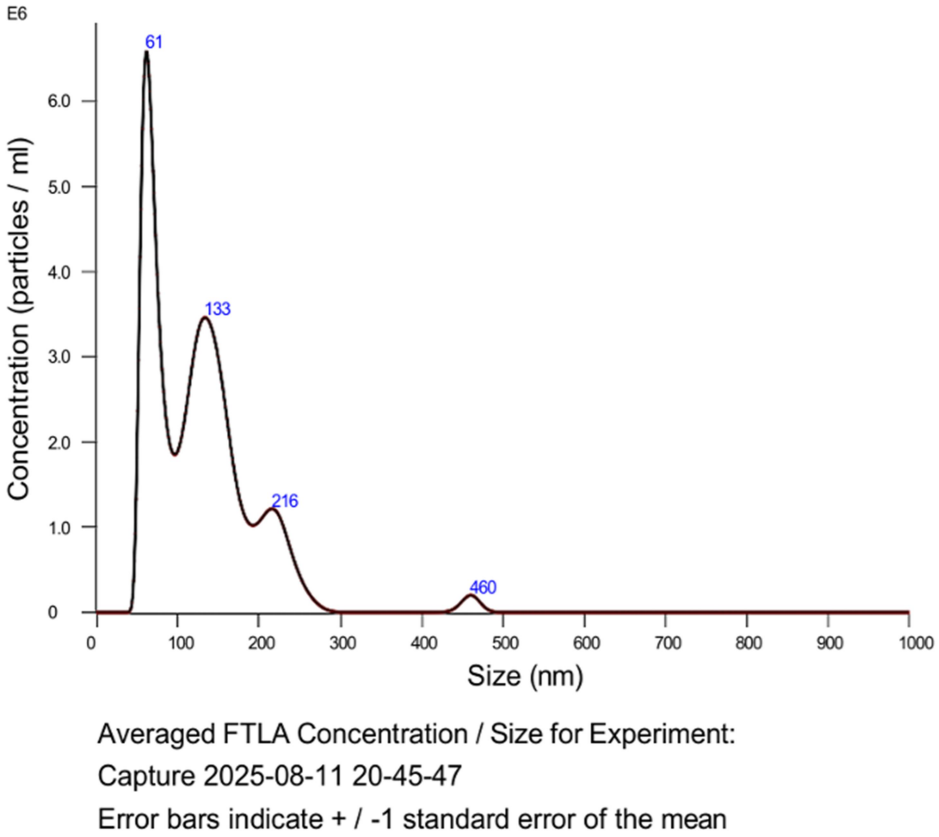

Figure 4: (Finite track length adjustment (FTLA) concentration/size image for Zno-B nanoparticle tracking analysis (NTA) Nanoparticle) with Filter

Table 1:

Results

Stats: Merged Data	
Mean:	162.2 nm
Mode:	60.7 nm
SD:	103.9 nm
D10:	57.9 nm
D50:	187.5 nm
D90:	263.9 nm
Stats: Mean +/- Standard Error	
Mean:	162.2 +/- 0.0 nm
Mode:	60.7 +/- 0.0 nm
SD:	103.9 +/- 0.0 nm
D10:	57.9 +/- 0.0 nm
D50:	187.5 +/- 0.0 nm
D90:	263.9 +/- 0.0 nm
Concentration:	1.44e+009 +/- 0.00e+000 particles/ml
	73.3 +/- 0.0 particles/frame
	210.4 +/- 0.0 centres/frame

Table 2:

Results

Stats: Merged Data	
Mean:	125.1 nm
Mode:	60.3 nm
SD:	65.2 nm
D10:	57.3 nm
D50:	117.6 nm
D90:	208.7 nm
Stats: Mean +/- Standard Error	
Mean:	125.1 +/- 0.0 nm
Mode:	60.3 +/- 0.0 nm
SD:	65.2 +/- 0.0 nm
D10:	57.3 +/- 0.0 nm
D50:	117.6 +/- 0.0 nm
D90:	208.7 +/- 0.0 nm
Concentration:	4.84e+008 +/- 0.00e+000 particles/ml
	24.6 +/- 0.0 particles/frame
	49.5 +/- 0.0 centres/frame

Zeta Potential Measurement:

Zeta potential, a crucial metric that may be used to assess the relative stability of various nanofluid types and identify the surface charge of a layer of nanoparticles, attracts oppositely charged ions. Upon contact between a solid nanoparticle surface and an aqueous solution, an interfacial charge layer is established, resulting in the reorganization of local free ions in the solution and generating a narrow area of non-zero charge at the interface. An electrical double layer and a thin layer of counterions to the charged solid surface are created by the rearrangement of charges at the solid-liquid interface and balancing counterions in the liquid. Strong electrostatic attraction makes the counterions in the contact layer stationary, while the counterions outside the compact layer are mobile. When the cadence is broken, charges become uncompensated, and the electron neutrality is lost, which causes the surface to become charged [19].

In a pure crystalline ionic solid, positive and negative charges are compensated because of the electron neutrality inside the lattice. Because of interaction, two layers are created throughout this process: the diffuse layer of mobile charges and the stern layer of stationary charges with regard to the particle surface and opposing charges. Stern potential is the difference in potential between the bulk solution and the outer edge of the stern layer. The electrostatic potential at the boundary between the diffuse and compact layers is known as the zeta potential.

The observed electrophoretic mobility of the probe particles is used to compute the zeta potential. Therefore, the speed and direction of the displacement of particles suspended in an aqueous ionic media measure the zeta potential, determined by the Kinetic Capillary Electrophoresis (KCE) [20]. A high absolute Zeta Potential indicates strong electrostatic repulsion between particles, which helps to keep them dispersed and prevents aggregation.

As seen in figures 6 and 8, the Zeta Potentials of the ZnO-A and ZnO-B samples measured by Zetasizer are 55.98 mV and 30.39 mV, respectively. This shows that the nanomaterial (ZnO-A) under evaluation is more stable, has high dispersity, inhibits aggregation (preventing the particles from clumping together), and bolsters the electrical properties of the composite than the nanomaterial (ZnO-B).

Mobility distribution versus Zeta Potential:

The mobility distribution shows the range of speeds at which nanoparticles move in an electric field, while the Zeta Potential is a calculated number that reflects a nanoparticle's surface charge and stability.

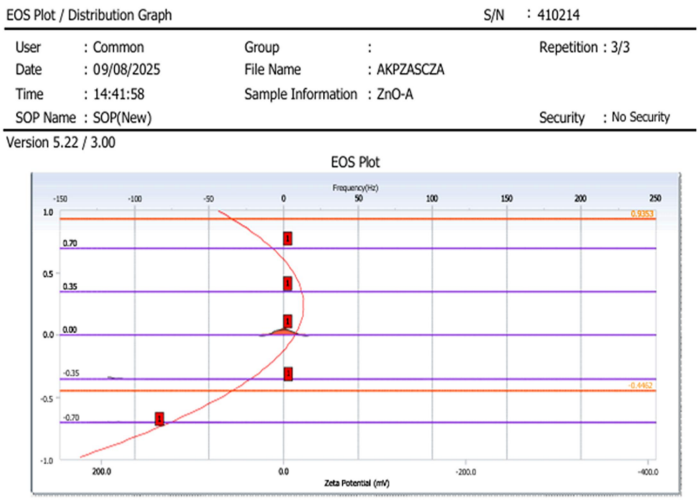

Figure 5: (Zeta potentials at different locations in a flat surface cell due to the total apparent electroosmotic flow of the probe particles, obtained during the measurement of the Zeta potential for a Zno-A Nanoparticles) with Filter

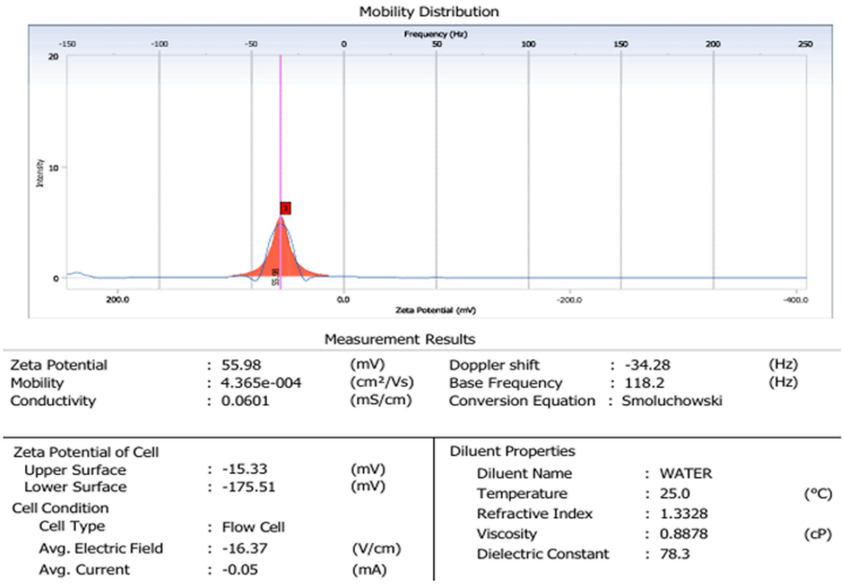

Figure 6: (Data of Zeta potential measurement of Zno-A Nanoparticles) with Filter

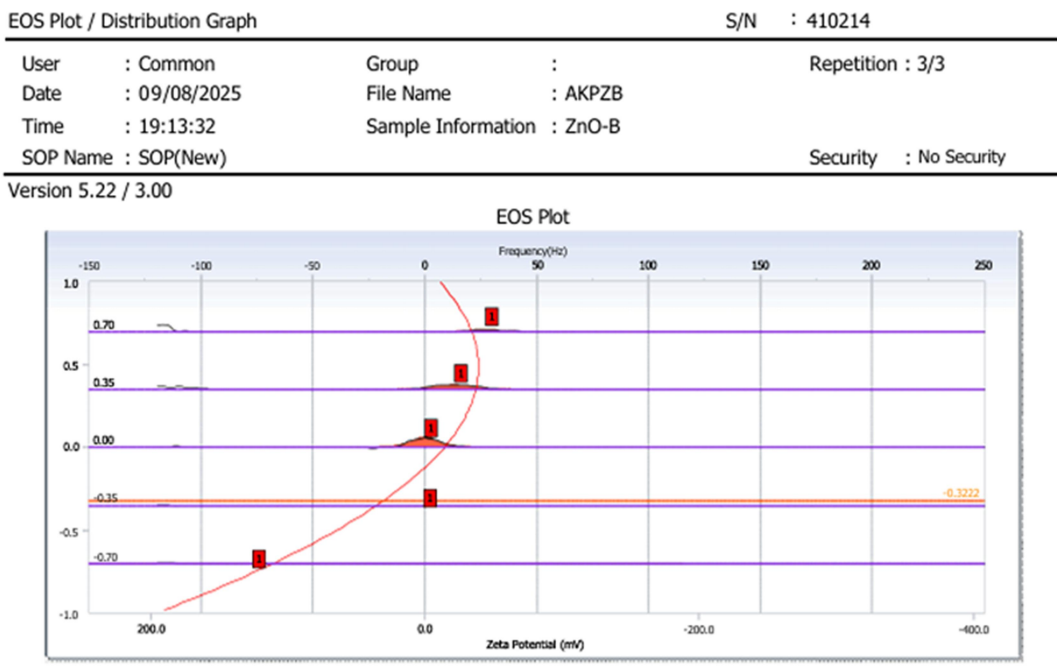

Figure 7: (Zeta potentials at different locations in a flat surface cell due to the total apparent electroosmotic flow of the probe particles, obtained during the measurement of the Zeta potential for a Zno-B Nanoparticles)

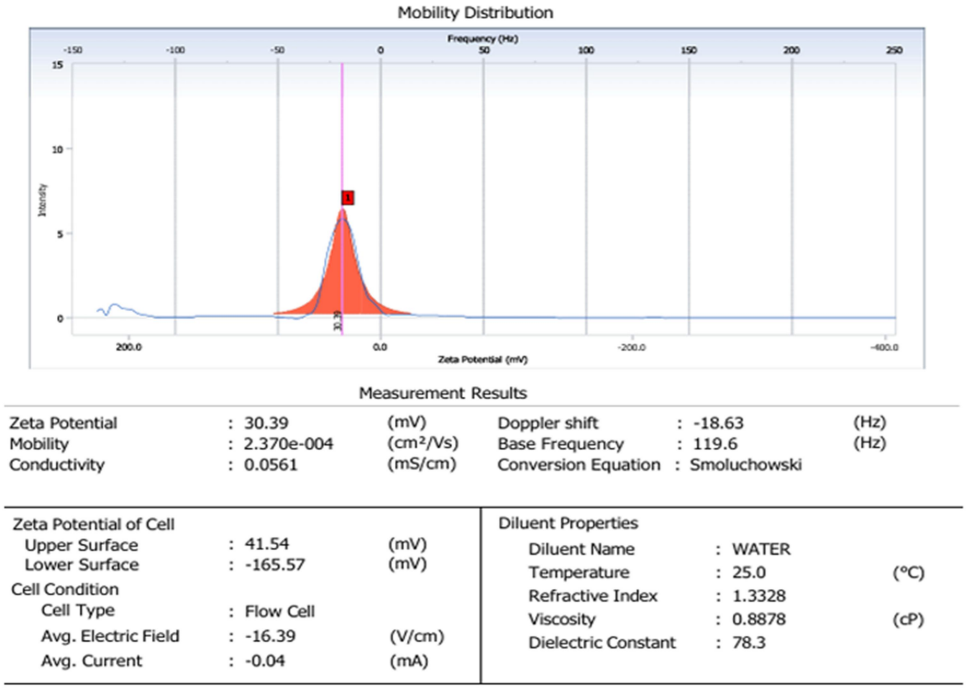

Figure 8: Zeta potential measurement of Zno-B Nanoparticles

The particle's mobility is assessed by electrophoretic velocity, which is the movement of a charged particle immersed in liquid under the influence of an external electric field [21]. Electrophoretic velocity per unit electric field strength (called particle mobility) is positive when it progresses towards a lower potential and negative when it travels towards a higher potential [22]. The mobility of ZnO-A nanoparticles under the influence of an electric field is 4.365×10^{-4}, more than that of ZnO-B nanoparticles, which was determined to be 2.370×10^{-4}. In materials doped with these nanoparticles, higher mobility of charge carriers, such as electrons or holes in ZnO-A relative to ZnO-B, suggests fewer scattering events and improved carrier transports. As a result, the ZnO-A nanoparticle-doped composite will have higher electrical conductivity than the ZnO-B-doped composite, as demonstrated by UV-treated (ZnO-A or ZnO-B) films, because doping with higher mobility (ZnO-A or ZnO-B) variants enhances applications such as transparent conductors or sensors, where mobility increases greatly, raising conductivity. This idea is applicable to nanoparticles ZnO-A and ZnO-B, associated polymer matrix (PVC) in the composites (PVC/ZnO-A and PVC/ZnO-B). By substantially improving carrier mobility and reducing oxygen traps at grain boundaries, UV treatment produces higher conductivity without sacrificing transparency [23].

Intensity versus Size graph:

The intensity versus size graph allows for the visualization of various particle populations within a polydisperse sample that may be resolved in a straightforward size distribution graph by plotting the intensity of light scattered by individual particles on one axis (intensity axis) against their measured size on another axis (size axis). As illustrated in figures 9 and 10, plots in the two dimensions (number or concentration axis) can display distinct subpopulations, with larger, brighter particles appearing higher on the intensity axis [24].

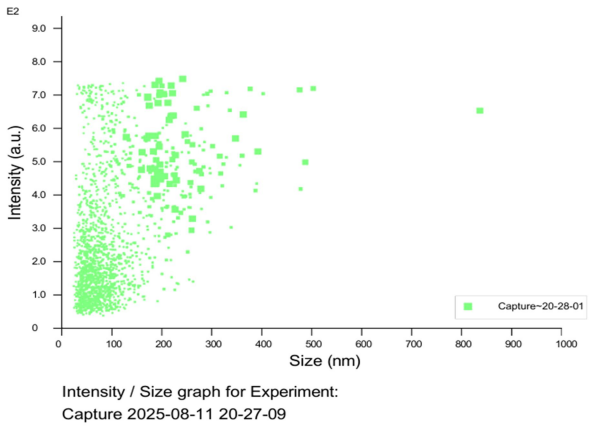

Figure 9: (Intensity - size plot of Zno-A nanoparticles)

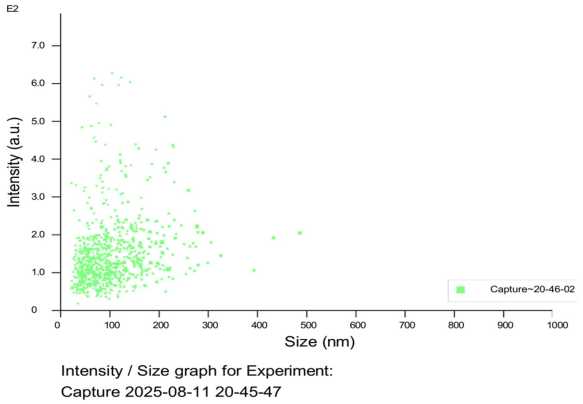

Figure 10: (Intensity - size plot of Zno-B nanoparticles)

The majority of nanoparticles in figure-10 are nearly the same size, while some of the nanoparticles in figure-9 are roughly the same size, but others are different.

Structural behavior of Polyvinyl Chloride (PVC) with incorporated ZnO nanoparticle:

When zinc oxide (ZnO-A and ZnO-B) nanoparticles are deposited in polyvinyl chloride (PVC), they alter the material's hydrophilicity and surface shape, which reduces the crystallization and increases amorphous regions, which changes the material's electrical and thermal stability. The material's performance is impacted by the structural modifications, which enhance PVC's mechanical and thermal resistance as well as its electrical and optical qualities.

When nanoparticles (ZnO-A and ZnO-B) are added to pure PVC, they greatly increase the hydrophilicity of PVC membranes by reducing the contact angle [25]. Additionally, they also produce larger surface pore diameters, higher porosity, and greater surface pore density, which improve PVC's heat resistance by preventing or delaying the breakdown of the polymer backbone.

Due to intermolecular interaction and charge transfer between zinc oxide (ZnO-A and ZnO-B) nanoparticles and Polymer polyvinylchloride (PVC) chains, the PVC matrix has now become more amorphous areas, a rougher, more porous surface morphology with different pore architectures, and higher glass transition temperature and heat stability [26, 27]. When the nanoparticles agglomerate at higher concentrations, the surface may become more brittle and rougher. The zinc oxide (ZnO-A and ZnO-B) nanoparticles and the polymer polyvinylchloride (PVC) generate a charge transfer complex that reduces the optical band gap of the nanocomposite [28].

Agglomeration of nanoparticles in PVC weakens the composite overall and produces poor mechanical and thermal properties by producing larger clusters that reduce the effective surface area and volume fraction of the nanoparticles. When nanoparticle clusters are present, the composite's thermal expansion coefficient may increase, making it more prone to expansion under heat. Nanoparticles function effectively, when they are widely dispersed and have a large surface area for interacting with the polymer matrix. Agglomeration reduces the specific surface area, and this reduced surface area limits the enhancement of the interfacial properties of the nanocomposite [29, 30].

Variation in the PVC/ZnO composite's dielectric constant as a function of temperature and frequency:

The dielectric constant, defined as the ratio of the capacitance with the material to that without the material, is a measure of the material's ability to retain electrical energy when an electric field is applied.

$$Dielectric\ Constant, \in_r = \frac{C}{C_o},$$

where C is the capacitance with the material and C_o that of without material.

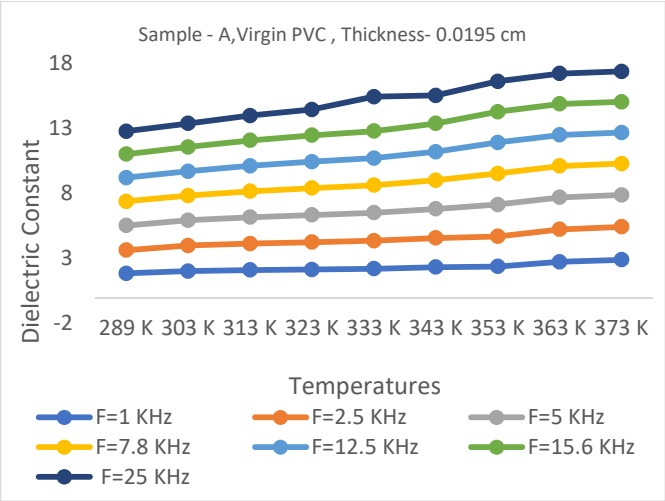

Figure 11: Temperature and frequency variations in the dielectric constant of the virgin sample of thickness 0.0195 cm.

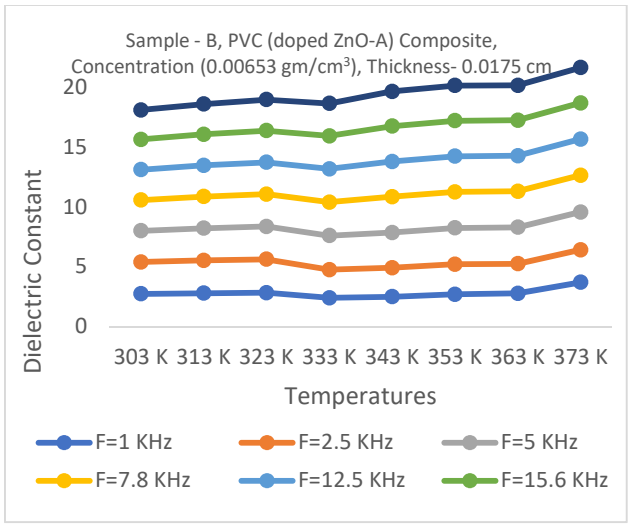

Figure 12: Temperature and frequency variations in the dielectric constant of the Composite doped with nanoparticles (PVC/ZnO-A) of thickness – 0.0175 cm

The composite (PVC/ZnO-A) doped with ZnO-A nanoparticles, as seen in figures 11, 12, 13, and 14, exhibits a gradual increase in dielectric constant when temperature is increased from 303K to 373K, due to increased thermal agitation of dipoles and charge carriers, intensifying polarization effects such as orientational and space charge distribution, which illustrate how the dielectric constant varies with temperature at constant frequency. The increased dipole mobility and interfacial polarization at high temperatures enable alignment with the electric field before relaxation time, which is the main factor responsible for the continuous rise. As a result, when torque is applied, dipoles gain rotational mobility to align with an electric field, minimizing the system's potential energy and increasing dielectric constant. The composite doped with ZnO-B nanoparticles, as shown in figures 15 and 16, first experiences a loss in dielectric constant between 303K and 313K because of rapid increase in heat agitation that causes a decrease in dipole alignment and randomize the dipole alignment. The dipole's inability to swiftly adjust to changes in the field causes the dielectric constant to drop. When molecular alignment is impeded at low temperature (between 303K to 313K), the dielectric constant usually drops because of the decreased thermal energy, which limits orientational polarization by assisting dipoles in orienting with an applied electric field.

At higher temperatures (313K – 323K or 333K – 343K), dipole dominance increases, and hence, the dielectric constant rises until the transition point. Thus, at all frequencies, a material's dielectric response is actively influenced by electronic, atomic, orientational (dipolar), and interfacial (space-charge) polarizations. The increased thermal energy in this temperature range causes PVC polymer chain dipoles to be more mobile, which enhances polarization and improves alignment with the applied electric field. ZnO-B nanoparticles in a composite (PVC/ZnO-B) raise the dielectric constant by interfacial polarization at the polymer-filler interfaces, where charge accumulation rises. The dielectric constant of the composite (PVC/ZnO-B) significantly decreases between 323K and 333K or 343K and 353K due to increased thermal agitation that disrupts the dipole alignment and interfacial polarization at the PVC/ZnO-B interface.

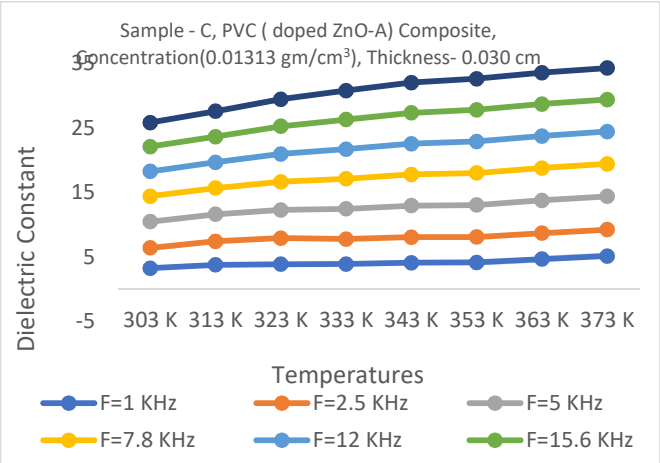

Figure 13: Temperature and frequency variations in the dielectric constant of the Composite doped with nanoparticles (PVC/ZnO-A) of thickness – 0.01313 cm.

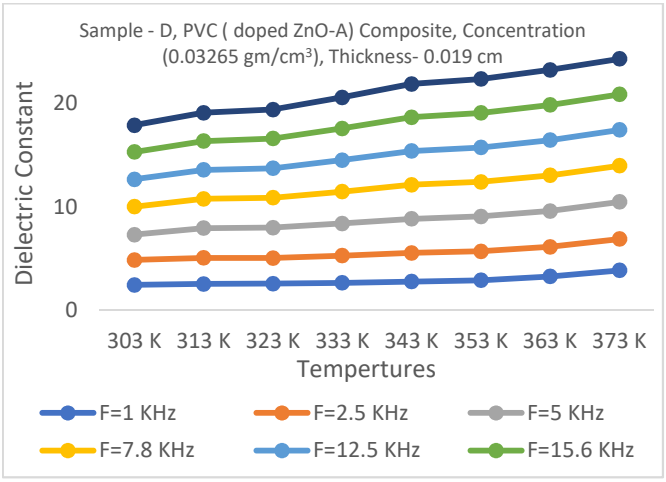

Figure 14: Temperature and frequency variations in the dielectric constant of the Composite doped with nanoparticles (PVC/ZnO-A) of thickness – 0.019 cm.

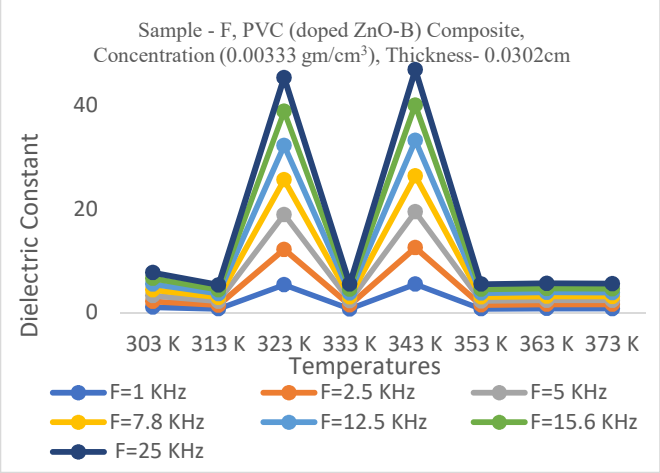

Figure 15: Temperature and frequency variations in the dielectric constant of the Composite doped with nanoparticles (PVC/ZnO-B) of thickness – 0.0302 cm.

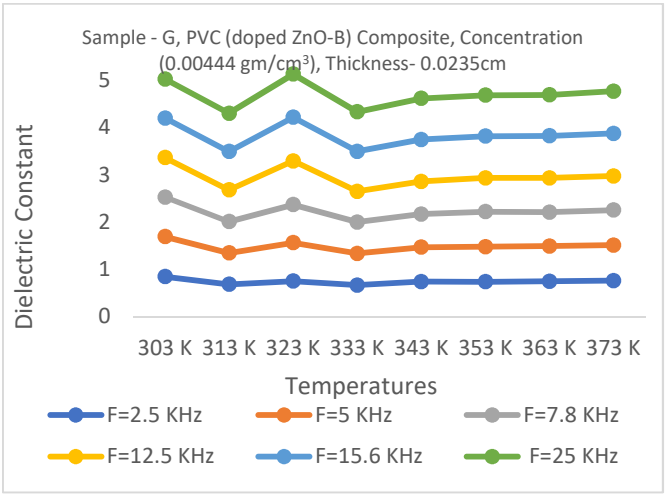

Figure 16: Temperature and frequency variations in the dielectric constant of the Composite doped with nanoparticles (PVC/ZnO-B) of thickness – 0.0235 cm.

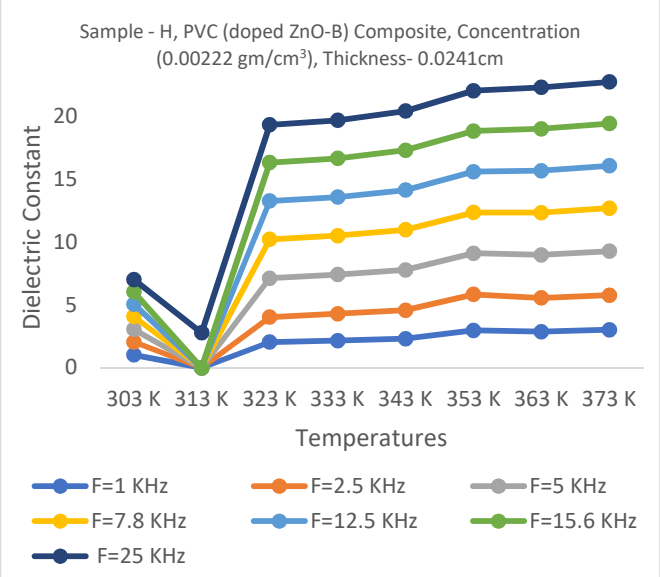

Figure 17: Temperature and frequency variations in the dielectric constant of the Composite doped with nanoparticles (PVC/ZnO-B) of thickness – 0.0241 cm.

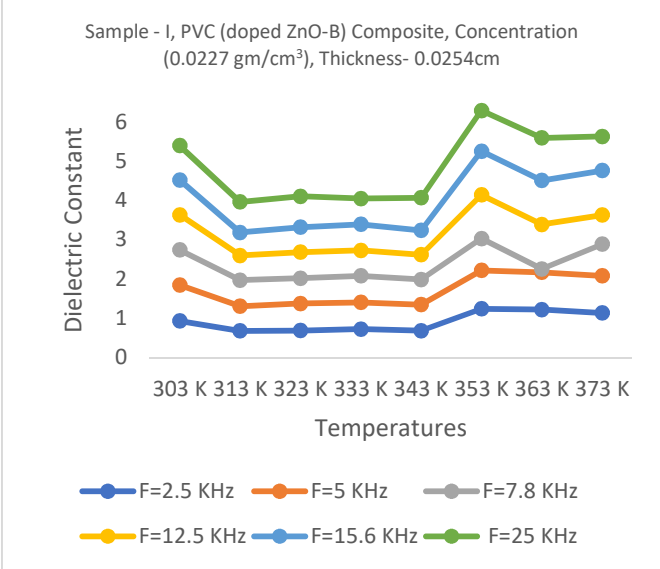

Figure 18: Temperature and frequency variations in the dielectric constant of the Composite doped with nanoparticles (PVC/ZnO-B) of thickness – 0.0254 cm.

Beyond a certain frequency, resonance in ionic or electronic polarization causes the dielectric constant to drastically decrease when the dipoles are unable to keep up with the applied field. Space charge and interfacial effects dominate at lower temperatures and lead to high dielectric values; however, as the temperature increases, thermal agitation reduces their effectiveness, causing a sharp decrease [31, 32, 33, 34]. The increased kinetic energy from rising temperatures causes dipoles to oscillate erratically and misalign with the applied electric field, reducing total polarization and, dielectric constant when spontaneous polarization collapses. This impact is more noticeable in materials that depend on orientational polarization, when field-induced ordering is overpowered by thermal motion. Because of increased orientational or dipolar polarization, the dielectric constant shows a "bump up" when temperatures rise at constant frequency [35, 36, 37, 38] within the temperature range of 343K and 353K. As the temperature rises from 353K to 373K, shown in figures 15 and 16, the dielectric constant stays constant because electronic polarization predominates, which is essentially temperature independent. At higher temperatures, contributions from other polarization mechanisms, such as orientational or space charge, decrease or saturate. Thermal agitation limits dipole alignment and interfacial polarization effects at high temperatures above 353K, resulting in a steady dielectric constant that is mostly controlled by electronic polarization and does not change much with temperature.

As shown in figure -17, when the temperature rises from 303K to 313K, dipole alignment under the electric field is disrupted due to increased thermal agitation. This lowers the dielectric constant by reducing interfacial or space charge polarization. The dielectric constant rises as a result of additional heating to 323K, which either strengthens intrinsic dipolar polarization or triggers other processes like electronic or orientational contributions. When different types of polarization complete polar material (like PVC) exhibit this behavior. This rise indicates structural alterations or decreased dipole cancellation from bond length expansions and rotations, whereas the initial drop is caused by dominant thermal disruption of dipoles. The initial thermal disruption effect is overcome by a greater contribution from space charge or interfacial polarization at higher temperatures, which accounts for the modest increase to 373K.

In the temperature (303K–313K) in figure 18, the increased thermal energy reduces orientation

polarization and lowers the dielectric constant by upsetting dipole alignment in the electric field. At these mild temperatures, thermal agitation predominates over other effects by randomizing dipole orientations. Plateau polarization finds an equilibrium where any new conductivity contributions are countered by thermal disorder, maintaining a steady dielectric constant at elevated temperatures of 313K to 343K.

Due to a small net shift in polarization mechanisms, the dielectric constant in the PVC/ZnO-B composite stabilizes at intermediate temperatures. Enhanced thermal activation causes a little increase in the dielectric constant between temperatures (343K and 373K) by increasing charge carrier mobility and interfacial or space charge polarization. At higher temperatures, this takes precedence over dipole randomization in the composite (PVC/ZnO-B). During these times, PVC/ZnO-B exhibits notable increase in the dielectric constant, which are probably caused by phase transitions, enhanced interfacial polarization, or nanoparticle agglomeration triggered at higher temperatures. PVC/ZnO-A, on the other hand, exhibits continuous increase, indicating a more uniform ZnO-A dispersion that permits constant dipole alignment and increasing conductivity with temperature. These characteristics are suitable for flexible electronics, temperature stable capacitors, and sensors, where controlled permittivity variations improve performance under thermal stress.

CONCLUSION

The Zeta Potential of the ZnO-A and ZnO-B samples tested by Zetasizer was found to be 55.98 mV and 30.39 mV, respectively, indicating that ZnO-A is more stable than ZnO-B, which strengthens the composite's electrical characteristics. Because ZnO-A is more stable than ZnO-B, the dielectric constant of the composite (PVC/ZnO-A) formed by nanoparticles (ZnO-A) increases continuously with temperature, whereas the dielectric constant of the composite (PVC/ZnO-B) formed by nanoparticles (ZnO-B) varies irregularly with temperature, indicating that composite PVC/ZnO-A is more useful than composite PVC/ZnO-B. The congruent peaks in size distribution graphs from unfiltered (scatter mode, depicted in figures 1 and 3) and filtered (fluorescence mode with optical filter, illustrated in figures 2 and 4), the Nanoparticle Tracking Analysis (NTA) measurements suggests that the synthesized nanoparticles are devoid of contaminants or impurities. From 313K to 323K and 333K to 343K, the dielectric constant of Composite PVC/ZnO-B increases more substantially, whereas that of Composite PVC/ZnO-A increases continuously. In certain ranges (313-323 K and 333 – 343 K), the dielectric behavior of PVC/ZnO composites exhibits clear temperature-dependent patterns. These trends are probably related to variations in ZnO nanoparticle types (A and B), such as size, shape, or dispersion quality. This can be used for specialized electronic applications. The significant dielectric constant jumps are seen in PVC/ZnO-B during those periods, which may be caused phase transitions, increased interfacial polarization, or the activation of nanoparticle agglomeration at higher temperatures. PVC/ZnO-A exhibits constant increases, indicating a more homogeneous ZnO-A dispersion that permits consistent dipole alignment and a rise in conductivity with heat. These characteristics are appropriate for temperature stable capacitors, sensors, or flexible electronics where performance under thermal stress is enhanced by controlled permittivity change (working range 313 – 343K). Thus ZnO-A provides dependable insulation, whereas PVC/ZnO-B may enable switchable electronics. Long term stability and optical agglomeration control may be the subject of future research.

Authors Contributions:

Aman Kumar: Conceptualization, Methodology, Investigation, Data Curation, Writing-Original Draft;
Kamar Tanbir: Data Curation, Formal Analysis;
Sanjeev Kumar: Methodology, Formal Analysis;
Sanjay Kumar Yadav: Writing- Review & Editing;
Rakesh Kumar Singh: Visualization, Supervision;
N. A. Karimi: Conceptualization, Resources, Supervision, Acquisition, Writing-Review and Editing.

The final draft of the work has been reviewed and approved by all authors.

Data Availability: The data samples have been requested in an acceptable manner.

Conflict of Interest: The authors declare that none of the research provided in this study would have

been impacted by any known financial or interpersonal conflicts.

Acknowledgement: We express our gratitude to Prof. (Dr.) Shankar Kumar, Head of the Postgraduate Department of Physics at Patna University, Patna; Prof. (Dr.) Alka, Principal, Patna Science College, Patna University, Patna; and also, thanks to the Head, Prof. (Dr.) Rakesh Kumar Singh, Aryabhata Knowledge University, Patna, for experimental support.

REFERENCES

1. Faiza A, Abraiz, et al. Improved PVC/ZnO nanocomposite insulation for high voltage and high temperature application. **Sci Rep.** 2023;13:31473. doi:10.1038/s41598-023-31473-3.
2. Yassin MT, et al. Facile green synthesis of zinc oxide nanoparticles with potential synergistic activity with common antifungal agents against multidrug-resistant candidal strains. **Crystals.** 2022;12(6):774. doi:10.3390/cryst12060774.
3. Al-Muntaser AA, Banoqitah E, et al. Fabrication and characterization of nano-composite flexible films of ZnO and poly(vinyl chloride)/poly(N-vinyl carbazole) polymers for dielectric capacitor. **Arab J Chem.** 2023;16:105171. doi:10.1016/j.arabjc.2023.105171.
4. Gaabour LH, Kholoud A, et al. Structural, optical and thermal properties of a PVDF/PVC blend containing ZnO nanoparticles. **J Inorg Organomet Polym Mater.** 2017. doi:10.1007/s12633-017-9617-y.
5. Farahbod F, Bagheri F, Madadpour F. Effect of solution content ZnO nanoparticles on thermal stability of polyvinyl chloride. **J Nanotechnol Eng Med.** 2013;4(2):021002. doi:10.1115/1.4025209.
6. Seansukato S, Alam G, et al. Fabrication and performance evaluation of a novel composite PVC–ZnO membrane for ciprofloxacin removal by polymer-enhanced ultrafiltration. **Polymers (Basel).** 2024;16:3551. doi:10.3390/polym16243551.
7. Patil H, Marathe K, et al. Studies in synthesis of nano-zinc oxide mixed PVC matrix membrane and its application for ibuprofen drug removal. **J Hazard Mater Adv.** 2023;9:100247. doi:10.1016/j.hazadv.2023.100247.
8. Rajendran R, Mani A, et al. Photocatalytic, antibacterial and anticancer activity of silver-doped zinc oxide nanoparticles. **J Saudi Chem Soc.** 2020. doi:10.1016/j.jscs.2020.10.008.
9. Yusof HM, Abdul Rahman NA, et al. Optimization of biosynthesis of zinc oxide nanoparticles: desirability-function-based response surface methodology, physicochemical characteristics and antioxidant properties. **MethodsX.** 2022. doi:10.1016/j.onano.2022.100106.
10. Mar A, et al. Study of electrical and optical properties of PVC composites filled with zinc oxide (ZnO) nanoparticles synthesized by sol-gel and dropwise mixing process. **Int J Nanotechnol Appl.** 2018;12(1):13-24.
11. Kumar A, Bhatt MK, Bhatt RJ, Karimi NA. Study on zinc oxide nanoparticles. **Bull Pure Appl Sci D Phys Sci.** 2010;29(2):161-167.
12. Kumar A, Karimi NA. Synthesis of zinc oxide nanoparticles by sol-gel method and dropwise mixing process. **J Surf Sci Technol.** 2015;31(3-4):179-183. doi:10.18311/jsst/2015/4397.
13. Kumar A. Study of optical properties of PVC/Ag_2O nanocomposites by dispersing spherical nanofillers into polymer matrix under normal and heat-treated conditions. **Bull Pure Appl Sci D Phys Sci.** 2023;42(1):35-45. doi:10.48165/bpas.2023.42D.1.3.
14. Wang Y, et al. A regularization algorithm of dynamic light scattering for estimating the particle size distribution of dual-substance mixture in water. **Particuology.** 2024. doi:10.1016/j.partic.2023.11.007.
15. Sun Z, Zhang J, Tong Z, Zhao X, et al. Particle size effects on the reflectance and negative polarization of light backscattered from natural surface particulate medium: Soil and sand. **J Quant Spectrosc Radiat Transf.** 2014;133:1-12. doi:10.1016/j.jqsrt.2013.03.013.
16. Markiewicz A, et al. Generation of nano- and micro-sized organic pollutant emulsions in simulated road runoff. **Environ Int.** 2019;133:105140. doi:10.1016/j.envint.2019.105140.
17. Malm AV, et al. Improved dynamic light scattering using an adaptive and statistically driven time-resolved treatment of correlation data. **Sci Rep.** 2019;9:13519. doi:10.1038/s41598-019-50077-4.
18. Maršálek R. Particle size and zeta potential of ZnO. **APCBEE Procedia.** 2014;9:13-17. doi:10.1016/j.apcbee.2014.01.003.

19. Serrano-Lotina A, et al. Zeta potential as a tool for functional materials development. **Catal Today.** 2023;423:113862. doi:10.1016/j.cattod.2022.08.004.
20. Rangamani P. Modelling spatio-temporal interactions within the cell. **J Biosci.** 2007;32(1):157-167.
21. Meléndrez MF, Cárdenas G, Arbiol J. Synthesis and characterization of gallium colloidal nanoparticles. **J Colloid Interface Sci.** 2010;346(2):279-287. doi:10.1016/j.jcis.2009.11.069.
22. Nie H, Jia J, She Y, Li M. Progress on pigment dispersion issues. **Pigment Resin Technol.** 2025. doi:10.1108/PRT-09-2024-0101.
23. Nguyen VH, et al. Increasing the electron mobility of ZnO-based transparent conductive films deposited by open-air methods for enhanced sensing performance. **ACS Appl Nano Mater.** 2018. doi:10.1021/acsanm.8b01745.
24. Senthilkumar N, et al. Synthesis of ZnO nanorods by one-step microwave-assisted hydrothermal route for electric device application. **J Mater Sci Mater Electron.** 2018;29. doi:10.1007/s10854-017-8223-5.
25. Arozal W, et al. Development, characterization and pharmacokinetic profile of chitosan-sodium tripolyphosphate nanoparticles based drug delivery systems for curcumin. **Adv Pharm Bull.** 2021;11(1):77-85. doi:10.34172/apb.2021.008.
26. de la Calle I, et al. Particle size characterization of Sepia ink eumelanin biopolymers by SEM, DLS and AF4-MALLS. **Food Anal Methods.** 2019. doi:10.1007/s12161-019-01448-0.
27. Peters RJB, et al. Evaluation of the performance of nanoparticle tracking analysis (NTA) for the measurement of nanoplastics. **Nano Converg.** 2025;12(2). doi:10.1186/s40550-025-00112-2.
28. Moloto W, Mbule P, Nxumalo E, Ntsendwana B, et al. Stabilizing effects of zinc(II)-benzene-1,3,5-tricarboxylate metal-organic frameworks on the performance of TiO_2 photoanodes for use in dye-sensitized solar cells. **J Photochem Photobiol A Chem.** 2021;407:113063. doi:10.1016/j.jphotochem.2020.113063.
29. Dananjaya SHS, et al. Synthesis, characterization of ZnO-chitosan nanocomposites and evaluation of its antifungal activity against pathogenic *Candida albicans*. **Int J Biol Macromol.** 2018;108:1281-1288. doi:10.1016/j.ijbiomac.2017.11.046.
30. Bharathi D, et al. Synthesis of zinc oxide nanoparticles (ZnO NPs) using pure bioflavonoid rutin and their biomedical applications: antibacterial, antioxidant and cytotoxic activities. **Res Chem Intermed.** 2019;45:2065-2078. doi:10.1007/s11164-018-03717-9.
31. Saikia R, et al. Antifungal efficacy of green-synthesized zinc oxide nanoparticles against *Fusarium* spp.: an in vitro study. **Plant Arch.** 2025;25(1):1027-1036. doi:10.51470/PLANTARCHIVES.2025.v25.no.1.154.
32. González-Fernández JV, Pinzón-Moreno DD, et al. Green method, optical and structural characterization of ZnO nanoparticles synthesized using leaves extract of *Moringa oleifera*. **J Renew Mater.** 2021. doi:10.32604/jrm.2021.017377.
33. Yedurkar S, Maurya C, Mahanwar P. Biosynthesis of zinc oxide nanoparticles using *Ixora coccinea* leaf extract—A green approach. **Open J Synth Theory Appl.** 2016;5(1):1-14. doi:10.4236/ojsta.2016.51001.
34. Ponnamma D, et al. Synthesis, optimization and applications of ZnO/polymer nanocomposites. **Mater Sci Eng C Mater Biol Appl.** 2019;98:1210-1240. doi:10.1016/j.msec.2019.01.081.
35. Gaur MS, et al. Thermally stimulated dielectric properties of poly(vinylidene fluoride)-zinc oxide nanocomposite. **J Therm Anal Calorim.** 2011. doi:10.1007/s10973-010-0901-1.
36. Kaur D, et al. Dielectric properties of ZnO-based nanocomposites and their potential applications. **Int J Opt.** 2021;2021:9950202. doi:10.1155/2021/9950202.
37. Rayssi C, El Kossi S, et al. Frequency and temperature dependence of dielectric permittivity and electric modulus studies of the solid solution. **RSC Adv.** 2018. doi:10.1039/C8RA00794B.
38. Faried M, Shameli K, et al. A green approach for the synthesis of silver nanoparticles using ultrasonic radiation times in sodium alginate media: Characterization and antibacterial evaluation. **J Nanomater.** 2016;2016:4941231. doi:10.1155/2016/4941231.